



J. Serb. Chem. Soc. 74 (11) 1259–1271 (2009)
JSCS–3916

Transition metal complexes with pyrazole-based ligands. Part 29. Reactions of zinc(II) and mercury(II) thiocyanate with 4-acetyl-3-amino-5-methylpyrazole

ŽELJKO K. JAĆIMOVIĆ¹, GORAN A. BOGDANOVIĆ², BERTA HOLLÓ^{3#},
VUKADIN M. LEOVAC^{3#} and KATALIN MÉSZÁROS SZÉCSÉNYI^{3*#}

¹Faculty of Metallurgy and Technology, Podgorica, Montenegro, ²“Vinča” Institute of Nuclear Sciences, Laboratory of Theoretical Physics and Condensed Matter Physics, Belgrade and ³Faculty of Sciences, Department of Chemistry, Novi Sad, Serbia

(Received 2 June, revised 4 October 2009)

Abstract: The work is concerned with the crystal and molecular structures of zinc(II) and mercury(II) complexes with 4-acetyl-3-amino-5-methylpyrazole (aamp) of the coordination formulae $[\text{Zn}(\text{NCS})_2(\text{aamp})_2]$ and $(\text{Haamp})_2[\text{Hg}(\text{SCN})_4]$. The zinc(II) complex was obtained by the reaction of a warm methanolic solution of aamp with a mixture of zinc(II) nitrate and ammonium thiocyanate, whereas the mercury(II) complex was prepared by the reaction of a warm ethanolic solution of aamp and a warm, slightly acidified aqueous solution of $[\text{Hg}(\text{SCN})_4]^{2-}$. Both complexes have a tetrahedral geometry, which in the case of zinc complex is formed by monodentate coordination of two aamp molecules and two isothiocyanate groups. The Zn(II) and Hg(II) atoms have significantly deformed coordination geometry. In both crystal structures the pyrazole derivative has a planar form, probably stabilized by an intramolecular N–H...O hydrogen bond. Apart from the X-ray structural analysis, the isolated complexes were characterized by elemental analysis, IR spectroscopy, conductometric measurements and thermal analysis.

Keywords: zinc(II) complex; mercury(II) complex; 4-acetyl-3-amino-5-methylpyrazole; crystal structure; thermal analysis.

INTRODUCTION

The focus of our research on transition metal complexes with pyrazole derivatives is due to the theoretical and practical significance of these compounds. A number of pyrazole derivatives show biological activity and, as a consequence, some are commercial products or compounds in the phase of activity evaluation. Their representatives show antipyretic,¹ antirheumatic² and antimicrobial³ be-

* Corresponding author. E-mail: mszk@uns.ac.rs

Serbian Chemical Society member.

doi: 10.2298/JSC0911259J

havior. Some of them are active ingredients of products with potential antitumor activity.^{4–6} In agriculture, they are in the use as pesticides.^{7–9} As pyrazoles readily form complexes, they are suitable agents for investigating the active sites of biomolecules¹⁰ and for modeling the biosystems of oxygen transfer.¹¹ In living organisms, metal ions are usually bonded to the imidazole part of histidine, which is a part of the proteins. In view of the similarity of pyrazole and imidazole,¹² they are suitable to mimic enzymatic reactions. From all the interesting pyrazole derivatives, our most intensive research is focused on the complexes of 4-acetyl-3-amino-5-methylpyrazole (aamp). This ligand exhibits outstanding complexing ability and, simultaneously, it displays considerable biological activity.¹³ The usual coordination mode of the aamp ligand is through its N2 (pyridine) nitrogen atom giving bis(aamp) complexes of the general formula $M(\text{aamp})_2X_2$.¹⁴ In basic solutions, *via* the deprotonated N1 atom, it acts as a bidentate bridging ligand giving bi- or polynuclear complexes.¹⁵ In a previous publications, the synthesis and structure of tetrahedral Zn(II) and Hg(II) complexes with the formula $[\text{Zn}(\text{NO}_3)_2(\text{aamp})_2]$ and $[\text{HgCl}_2(\text{aamp})_2]$ were described.¹⁶ Herein, the synthesis, crystal and molecular structure, as well as physicochemical properties of the complexes with the same central atoms and aamp ligand of the formulae $[\text{Zn}(\text{NCS})_2(\text{aamp})_2]$ and $(\text{Haamp})_2[\text{Hg}(\text{SCN})_4]$ are presented.

EXPERIMENTAL

Synthesis

In a previous work,¹⁷ the synthesis of $[\text{Zn}(\text{NCS})_2(\text{aamp})_2]$ was described but the resulting crystals were not suitable for X-ray structural analysis. Crystals of the same compound appropriate for X-ray analysis were obtained from MeOH solutions according to the following procedure. A mixture of 0.50 mmol $\text{Zn}(\text{NO}_3)_2 \cdot 6\text{H}_2\text{O}$ and 1.2 mmol NH_4NCS was dissolved in 8.0 cm³ of MeOH. The ligand (1.0 mmol) was dissolved in 8.0 cm³ of warm MeOH. The two solutions were mixed together and left to crystallize at room temperature for seven days. The white prismatic crystals were filtered off, washed with MeOH and air-dried. Yield: 61 %. Anal. Calcd. for $\text{ZnC}_{14}\text{H}_{18}\text{N}_8\text{O}_2\text{S}_2$ (459.88 g mol⁻¹): C, 36.56; H, 3.95; N, 24.37; S, 13.94 %. Found: C, 36.52; H, 3.90; N, 24.38; S, 13.92 %.

$(\text{Haamp})_2[\text{Hg}(\text{SCN})_4]$ was obtained as follows: 0.20 mmol $\text{Hg}(\text{SCN})_2$ and 0.50 mmol NH_4NCS were dissolved in 3 cm³ of water and one drop of *cc.* HCl was added. The ligand aamp (0.50 mmol) was dissolved in 3 cm³ of warm EtOH, and the warm solutions were mixed together. After two days standing at room temperature, the formed white, plate crystals were filtered off, washed with EtOH and air-dried at room temperature. Yield: 44 %. Anal. Calcd. for $\text{HgC}_{16}\text{H}_{20}\text{N}_{10}\text{O}_2\text{S}_4$ (713.26 g mol⁻¹): C, 26.94; H, 2.83; N, 19.64; S, 17.98 %. Found: C, 26.90; H, 2.80; N, 19.65; S, 18.00 %.

Elemental analysis data were obtained by standard methods.

FT-IR data were collected at room temperature as KBr pellets, in the range 4000–400 cm⁻¹ using a Thermo Nicolet (NEXUS 670 FT-IR) spectrophotometer.

Molar conductivities of freshly prepared 1.0 mmol dm⁻³ solutions were measured on a Jenway 4010 conductivity meter.

X-Ray experiments and crystal structure determination

Single-crystal X-ray diffraction data for $(\text{Haamp})_2[\text{Hg}(\text{SCN})_4]$ were collected on an Enraf-Nonius CAD-4 diffractometer¹⁸ using $\text{MoK}\alpha$ radiation ($\lambda = 0.71069 \text{ \AA}$) and $\omega/2\theta$ scans in the 2θ range from 1.67 to 29.96° . The cell constants and an orientation matrix for data collection, obtained from 24 centered reflections in the range 12.10 – 16.82° , corresponded to a monoclinic cell, the dimensions of which are given in Table I. The data were corrected for Lorentz and polarization effects.¹⁹ A Gaussian-type absorption correction^{20–22} based on the crystal morphology was applied ($T_{\min} = 0.217$; $T_{\max} = 0.354$).

TABLE I. Crystallographic data for the compounds $[\text{Zn}(\text{NCS})_2(\text{aamp})_2]$ and $(\text{Haamp})_2[\text{Hg}(\text{SCN})_4]$

Property	$[\text{Zn}(\text{NCS})_2(\text{aamp})_2]$	$(\text{Haamp})_2[\text{Hg}(\text{SCN})_4]$
Empirical formula	$\text{C}_{14}\text{H}_{18}\text{ZnN}_8\text{O}_2\text{S}_2$	$\text{C}_{16}\text{H}_{20}\text{HgN}_{10}\text{O}_2\text{S}_4$
Formula weight	459.85	713.26
Crystal size, mm^3	$0.28 \times 0.25 \times 0.10$	$0.18 \times 0.25 \times 0.35$
Crystal color/shape	White/plate	White/prism
Temperature, K	293(2)	293(2)
Wavelength, \AA	0.71069	0.71069
Crystal system	Triclinic	Monoclinic
Space group	<i>P1</i>	<i>C2/c</i>
Unit cell dimensions		
$a / \text{\AA}$	8.3466(4)	10.055(2)
$b / \text{\AA}$	10.8641(5)	10.379(3)
$c / \text{\AA}$	12.4718(5)	24.442(4)
$\alpha / ^\circ$	74.927(4)	90
$\beta / ^\circ$	88.563(4)	92.49(2)
$\gamma / ^\circ$	68.802(4)	90
$V / \text{\AA}^3$	1015.13(8)	2548.4(10)
Z	2	4
$D_{\text{calc}} / \text{g cm}^{-3}$	1.504	1.859
Absorption coefficient, mm^{-1}	1.442	6.402
Theta range for data collection ($^\circ$)	3.01–28.86	1.67–29.96
Index ranges	$-11 \rightarrow h \rightarrow 10$, $-13 \rightarrow k \rightarrow 14$, $-16 \rightarrow l \rightarrow 16$	$-14 \rightarrow h \rightarrow 14$, $0 \rightarrow k \rightarrow 14$, $0 \rightarrow l \rightarrow 34$
Reflections collected	10022	3785
Independent reflections	4638 ($R(\text{int}) = 0.017$)	3704 ($R(\text{int}) = 0.0237$)
Data/parameters	4638/248	3704/150
Goodness-of-fit on F^2	0.991	1.037
Final R indices [$I > 2\sigma(I)$]	$R_1 = 0.0307$, $wR_2 = 0.0752$	$R_1 = 0.0416$, $wR_2 = 0.1078$
Largest diff. peak and hole, e \AA^{-3}	0.368 and -0.410	0.703 and -0.813

A single white crystal of $[\text{Zn}(\text{NCS})_2(\text{aamp})_2]$ was selected and glued on glass fiber. X-Ray diffraction data were collected on an Oxford Diffraction Gemini S four-circle diffractometer equipped with a Sapphire CCD detector. The crystal to detector distance of 45.0 mm and graphite monochromated $\text{MoK}\alpha$ ($\lambda = 0.71073 \text{ \AA}$) were used. X-Radiation were employed

in the measurement. The data were reduced using the Oxford Diffraction program Crys-Alis^{Pro}.²³ A semi-empirical absorption correction based upon the intensities of equivalent reflections was applied, and the data were corrected for Lorentz, polarization, and background effects.²³ Crystallographic data are given in Table I.

Both structures were solved by heavy atom²⁴ and difference Fourier methods and refined on F^2 by the full-matrix least-squares method.²⁴ All H atoms were placed at the calculated positions and they were refined with isotropic displacement parameters set to 1.2 times (1.5 for methyl groups) the equivalent isotropic U value of the parent atom. The software used to prepare the material for publication: PARST²⁵ and WinGX.²¹ Molecular graphics: ORTEPIII.²⁶ Crystallographic details are given in Table I.

Thermal analysis

Thermal measurements were performed on a Q600 SDT TA Instruments thermal analyzer. Simultaneous TG-DTA curves were obtained using alumina crucibles with sample masses of about 2 mg with an empty crucible serving as the reference. The heating rate was 20 °C min⁻¹ in flowing nitrogen and air gas carriers. Flow rate: 100 cm³ min⁻¹.

RESULTS AND DISCUSSION

Synthesis and selected physicochemical properties of the compounds

Single crystals of the Zn(II) complex were obtained by the reaction of warm, dilute methanolic solutions of the aamp ligand and a mixture of Zn(NO₃)₂·6H₂O and NH₄NCS in a mole ratio of 1:0.5:1.2.

The Hg(II) complex resulted from the reaction of warm ethanolic solution of the ligand and a warm, slightly acidic aqueous solution of Hg(SCN)₂ and NH₄NCS in a mole ratio of 1:0.4:1; hence, it was in fact the reaction between [Hg(SCN)₄]²⁻ and aamp. In view of the high stability of [Hg(SCN)₄]²⁻, *i.e.*, the strong Hg-S bond, as well as the solution acidity, it is not surprising that it was possible to isolate [Hg(SCN)₄]²⁻ containing two Haamp⁺ as counter ions.

It should be mentioned that an attempt to prepare a mixed-ligand complex, *i.e.*, [Hg(SCN)₂(aamp)₂], in the same way as for the zinc(II) complex, was unsuccessful, as it resulted in the crystallization of the free ligand.

Both crystals were stable at room temperature. They were slightly soluble in water, EtOH and MeOH, but well soluble in DMF. The molar conductivity data of the colorless solutions of the Zn(II) and Hg(II) complexes, Λ_M , in DMF were 32 and 114 S cm² mol⁻¹, respectively. The value of the molar conductivity of [Zn(NCS)₂(aamp)₂] was somewhat larger than that for the non-electrolytes, which refers to the partial replacement of the NCS group with solvent molecules. The value of Λ_M of the (Haamp)₂[Hg(SCN)₄] complex is in agreement with its coordination formula and corresponds to a 2:1 electrolyte type.²⁷

In the IR spectra of the complexes, the thiocyanato group is identified by its very intensive bands, which appear at 2064 and 2082 cm⁻¹ (Zn-NCS) and 2099 and 2123 cm⁻¹ (Hg-SCN). The position of these bands agrees very well with the coordination mode of the corresponding group.²⁸

Molecular and crystal structures

Structure of $(\text{Haamp})_2[\text{Hg}(\text{SCN})_4]$. The structure of the $(\text{Haamp})_2[\text{Hg}(\text{SCN})_4]$ complex is presented in Fig. 1. In the unit cell, the Hg atom lies on a two-fold axis of symmetry (the second half of the complex anion and the other counter cation requires the symmetry operation $-x, y, -z + 1/2$). The two crystallographically different SCN groups have very similar bond distances (Table II). The nitrogen atoms from the two coordinated SCN groups participate in cyclic hydrogen bonds (Fig. 2) to the neighboring Haamp^+ ($\text{N1-H}\cdots\text{N4b}$ and $\text{N2-H}\cdots\text{N4a}$ hydrogen bonds in Table III). These hydrogen bonds influence the geometry of the complex anion and the mutual orientation of the SCN ligands with an $\text{N4a}\cdots\text{N4b}$ distance of only 3.31 Å. A search of the Cambridge Structural Database²⁹ for all crystal structures possessing an Hg atom with two or more bonded SCN ligands revealed that none of 72 Hg compounds had such a short $\text{N}\cdots\text{N}$ distance (less than 3.5 Å) for two coordinated SCN groups as exists in the complex studied herein. Another consequence of the observed cyclic H-bonds is that the C7b-S1b-Hg angle is bent to a value of $95.8(1)^\circ$, which is rather different from the expected, much higher value. It is noteworthy that such a low value of the C-S-Hg angle is also quite rare in the above mentioned 72 crystal structures found in the CSD database, although the Hg atom has four equivalent ligands. The S-Hg-S coordination angles are also very deformed and have the values over a rather wide range, from 102.3 to 114.8° (Table II). All this demonstrates the importance of intermolecular hydrogen bonds for the geometry of $[\text{Hg}(\text{SCN})_4]^{2-}$ and probably may be applied to similar tetrahedral molecules $[\text{ML}_4]$ that form intermolecular interactions through coordinated SCN groups. In other words, the mutual orientation of the ligands and the coordination angles could be significantly deformed due to intermolecular hydrogen bonds.

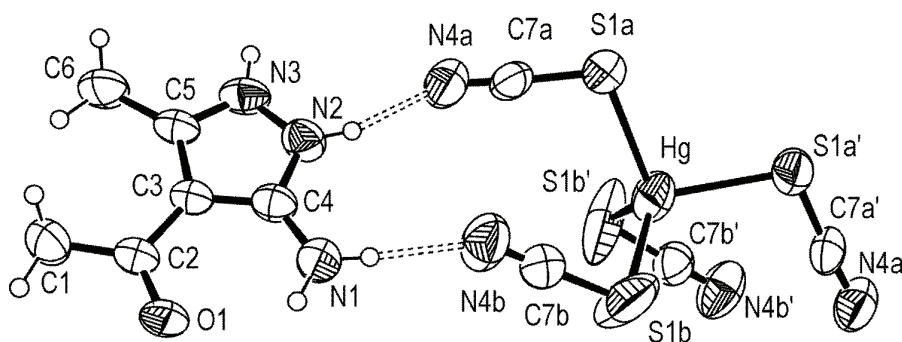


Fig. 1. The molecular geometry and atom labeling scheme of $(\text{Haamp})_2[\text{Hg}(\text{SCN})_4]$. The displacement ellipsoids are drawn at the 40 % probability level for non-H atoms. (The second half of the complex anion and the other counter cation requires the symmetry operation $-x, y, -z + 1/2$).

TABLE II. Selected Selected bond distances (Å) and angles (°) for [Zn(NCS)₂(aamp)₂] and (Haamp)₂[Hg(SCN)₄]. Symmetry code: (i) $-x, y, -z + 1/2$

[Zn(NCS) ₂ (aamp) ₂]			
Zn–N4a	1.9415(18)	N4a–Zn–N4b	114.10(9)
Zn–N4b	1.9537(19)	N4a–Zn–N2b	111.49(7)
Zn–N2b	2.0083(15)	N4b–Zn–N2b	109.04(7)
Zn–N2a	2.0124(16)	N4a–Zn–N2a	104.58(7)
S1a–C7a	1.603(2)	N4b–Zn–N2a	110.52(8)
N4a–C7a	1.152(3)	N2b–Zn–N2a	106.82(6)
S1b–C7b	1.608(2)		
N4b–C7b	1.143(3)		
(Haamp) ₂ [Hg(SCN) ₄]			
Hg–S1a	2.5386(15)	S1b ⁱ –Hg–S1b	114.8(2)
Hg–S1b	2.534(2)	S1b ⁱ –Hg–S1a ⁱ	108.00(7)
S1a–C7a	1.639(6)	S1b–Hg–S1a ⁱ	111.55(8)
N4a–C7a	1.150(7)	S1b ⁱ –Hg–S1a	111.55(8)
S1b–C7b	1.621(6)	S1b–Hg–S1a	108.00(7)
N4b–C7b	1.123(7)	S1a ⁱ –Hg–S1a	102.31(7)

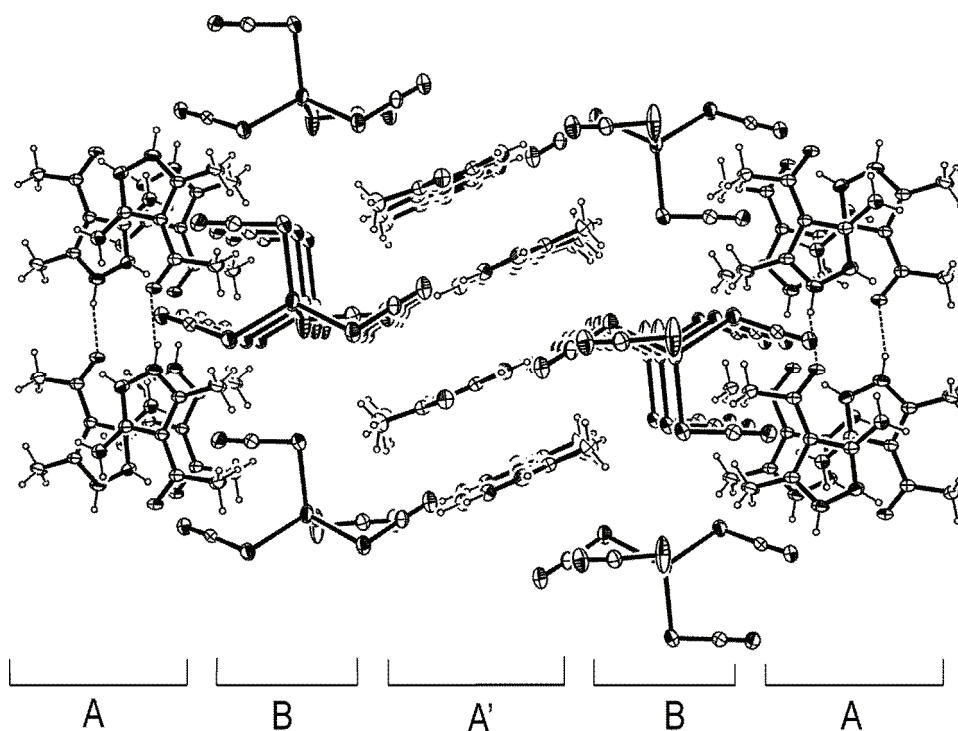
Fig. 2. The crystal lattice fragment of (Haamp)₂[Hg(SCN)₄] viewed down the $[-1, 1, 0]$ direction showing the mutual orientation of the complex anions and the pyrazolium cations.

TABLE III. The geometry of possible hydrogen bonds and selected intermolecular interactions for $(\text{Haamp})_2[\text{Hg}(\text{SCN})_4]$. Symmetry codes: (i) x, y, z ; (ii) $x-1/2, +y+1/2, +z$; (iii) $x+1/2, +y-1/2, +z$; (iv) $-x, -y, -z+1$

Bond	D–H (Å)	D···A (Å)	H···A (Å)	D–H···A (°)
N1–H1b···O1 ⁱ	0.86	2.787(5)	2.22	123
N1–H1a···N4b ⁱ	0.86	2.856(7)	2.00	175
N1–H1b···N4a ⁱⁱ	0.86	3.283(7)	2.56	142
N2–H2···N4a ⁱ	0.86	2.846(7)	2.03	159
N3–H3···O1 ⁱⁱⁱ	0.86	2.750(5)	1.92	164
C6–H6C···S1a ^{iv}	0.96	3.670(6)	2.81	149

All the non-hydrogen atoms in Haamp^+ are approximately coplanar, which is probably due to the delocalization of the π -electrons within the pyrazole ring and the weak π -bonding between the C2 and C3 atoms (the C2–C3 bond has a partial double bond character). Another reason for this could be the existence of an intramolecular N1–H1b···O1 hydrogen bond (Table III), which favors the coplanar position of the C1–C2–O1 fragment to the rest of molecule. Quite similar molecular planarity, including the observed intramolecular N–H···O hydrogen bond, was observed in other crystal structures of metal(II) complexes with aamp.^{14–16,30}

The crystal packing, shown in Fig. 2, consists of two types of layers. Layer A is composed of Haamp^+ arranged in parallel tapes with a mutual distance between the tapes (Haamp^+ planes) of approximately 3.3 Å. Inside of the tapes, the cations are interconnected by strong N3–H3···O1 hydrogen bonds (Table III). Layers A and A' are of the same composition and mutual orientation of the protonated ligands, but have an orthogonal orientation to each other. Layer B consists of $[\text{Hg}(\text{SCN})_4]^{2-}$ which interconnect the neighboring Haamp^+ from layers A and A' by strong N–H···N4 hydrogen bonds (Table III). Consequently, each complex anion (through its terminal nitrogen atoms) participates in four relatively strong hydrogen bonds. Additionally, N4a forms another (weak) hydrogen bond, while the S1a atom participates in a very weak C–H···S hydrogen bond, which deserves to be noted because of its relatively short H···S distance (Table III).

Crystal structure of $[\text{Zn}(\text{NCS})_2(\text{aamp})_2]$. A tetrahedral arrangement, most common in Zn(II) complexes, is established by the coordination of two NCS groups and two monodentate pyrazole ligands, which are, like in the majority of other structures, coordinated in the neutral form (Fig. 3). In contrast to the Hg(II) complex, where the thiocyanato groups are coordinated through the sulfur atom, the coordinating atoms in the Zn(II) complex are the nitrogens of the same group, which is in accordance with the Hard and Soft Acid and Base (HSAB) principle.^{31,32} However, the bond distances in the thiocyanato ligands are very similar in both complexes, with the S1–C7 bond being negligibly shorter in the Zn(II) complex than that in the Hg(II) complex. The N4–C7 bond lengths are practically the same in both compounds. Similarly to the Hg(II) complex, the coordination

angles are significantly deformed and vary in the 104.6–114.1° range (Table II). The widest angle, N4a–Zn–N4b, involve N atoms from the coordinated NCS groups.

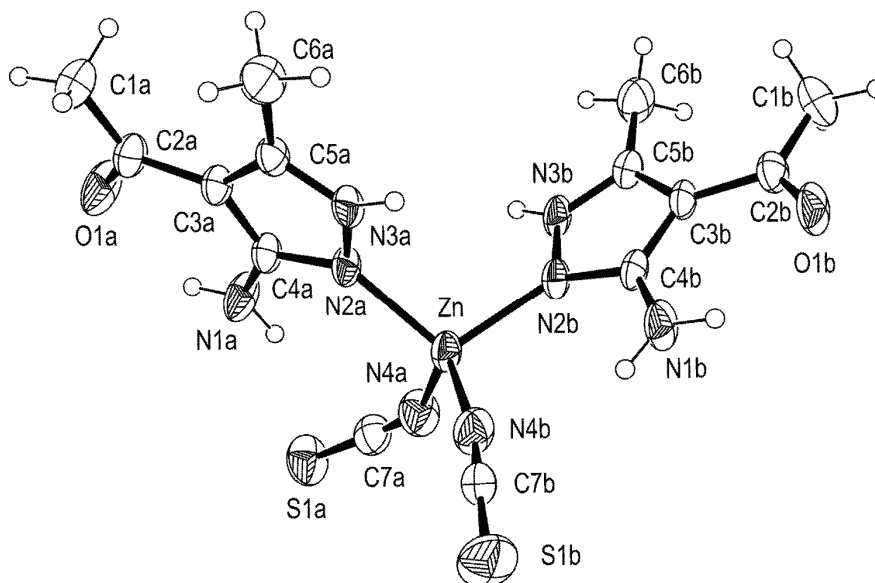


Fig. 3. The molecular geometry and atom labeling scheme of $[\text{Zn}(\text{NCS})_2(\text{aamp})_2]$. The displacement ellipsoids are drawn at the 40 % probability level for non-H atoms.

Despite the differences between the pyrazole derivatives in the two complexes, the analysis showed that the corresponding bond lengths are very similar (Table IV). The greatest deviation was observed in the N2–N3 bond length, which is shorter in the Hg(II) complex. The conformation of aamp is also very similar in both compounds. Namely, it has the same planar form, supported by possible N1–H···O1 intramolecular hydrogen bonds (Table V).

TABLE IV. A comparison of the bond distances (Å) in the pyrazole ligand for $[\text{Zn}(\text{NCS})_2(\text{aamp})_2]$ and $(\text{Haamp})_2[\text{Hg}(\text{SCN})_4]$

Bond	$[\text{Zn}(\text{NCS})_2(\text{aamp})_2]$		$(\text{Haamp})_2[\text{Hg}(\text{SCN})_4]$
	Ligand A	Ligand B	
O1–C2	1.233(2)	1.228(2)	1.233(5)
N1–C4	1.349(2)	1.339(2)	1.332(7)
N2–C4	1.334(2)	1.343(2)	1.339(6)
N2–N3	1.374(2)	1.379(2)	1.349(6)
N3–C5	1.313(2)	1.313(2)	1.324(6)
C2–C3	1.446(2)	1.438(2)	1.452(6)
C3–C4	1.403(2)	1.398(2)	1.405(7)
C3–C5	1.414(3)	1.420(3)	1.413(6)

TABLE V. The geometry of possible hydrogen bonds and selected intermolecular interactions for $[\text{Zn}(\text{NCS})_2(\text{aamp})_2]$. Symmetry codes: (i) x, y, z ; (ii) $-x+1, -y, -z+1, +z$; (iii) $-x+2, -y+1, -z, +z$; (iv) $-x+2, -y, -z+1$; (v) $-x+2, -y, -z$

Bond	D–H (Å)	D···A (Å)	H···A (Å)	D–H···A (°)
N1a–H1a2···O1a ⁱ	0.86	2.801(2)	2.23	124
N1a–H1a2···S1a ⁱⁱ	0.86	3.629(2)	2.83	154
N1a–H1a1···N4a ⁱ	0.86	3.128(2)	2.37	148
N1b–H1b2···O1a ⁱ	0.86	2.738(3)	2.16	125
N1b–H1b2···S1b ⁱ	0.86	3.638(2)	2.86	152
N1b–H1b1···N4b ⁱ	0.86	3.327(3)	2.57	147
N1a–H3a···O1b ⁱⁱⁱ	0.86	2.714(2)	1.86	174
N1b–H3b···O1a ^{iv}	0.86	2.769(2)	1.92	168
C1a–H1a5···S1b ^v	0.96	3.722(3)	2.87	148
C6a–H6a2···S1b ^v	0.96	3.684(3)	2.91	139

It is interesting to note that the oxygen atom of the pyrazole moiety forms the same H-bonds in both complexes. In addition to the already mentioned N1–H···O1 intramolecular H-bond, O1 participates in intermolecular N3–H···O1 H-bonds with very similar geometric parameters (Tables III and V). This is the strongest H-bond in the complexes, and it enables the chain formation, connecting the aamp molecules (Fig. 4). In the Zn(II) complex, the chains are additionally connected *via* weak C–H···S hydrogen bonds (Table V).

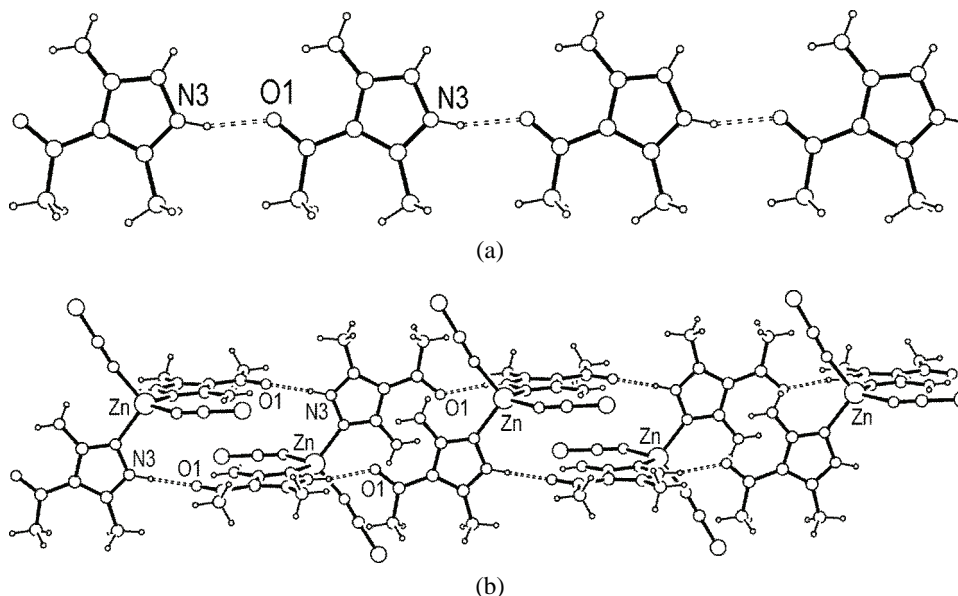


Fig. 4. In both crystal structures, the pyrazole derivatives form chains through the N3–H···O1 hydrogen bonds. The crystal lattice fragments for $(\text{Haamp})_2[\text{Hg}(\text{SCN})_4]$ and $[\text{Zn}(\text{NCS})_2(\text{aamp})_2]$ are illustrated in (a) and (b), respectively.

Thermal data

The thermal decomposition of $[\text{Zn}(\text{NCS})_2(\text{aamp})_2]$ has already been described.¹⁷ The repeated measurements have confirmed the former findings. According to the completely different crystal and molecular structure of the Hg(II) complex, its decomposition pattern is also different. The thermal stability of the Hg(II) compound is significantly lower compared to that of the zinc(II) complex (onset temperatures: 150 and 240 °C, respectively) and TG curve is continuous in the whole temperature range. As all four thiocyanato N4 atoms form relatively strong H-bonds with the neighboring Haamp⁺, it is reasonable to expect the departure of two HNCS molecules at the first decomposition step, which would be in accordance, within the experimental error, with the mass loss to the first minimum in DTG curve: 12.9 % (calcd. 16.57 %). Namely, according to the HSAB principle the interactions between the soft Hg(II) acid and the soft sulfur atom of the SCN⁻ base are remarkable. Therefore it is highly unlikely the loss of all four thiocyanato groups at the same time. With the loss of two HSCN molecule the Hg(II) analogue of the Zn(II) complex with a tentative composition of $\text{Hg}(\text{NCS})_2(\text{aamp})_2$ would be formed. The shape of the DTG curve may also support this proposition. However, it can be seen in Fig. 5 that the fragmentation of the organic part takes place simultaneously. The course of the decomposition is almost independent of the gas carrier up to 400 °C. Due to the high volatility of mercury, at higher temperatures, the oxidation of the organic fragments is ac-

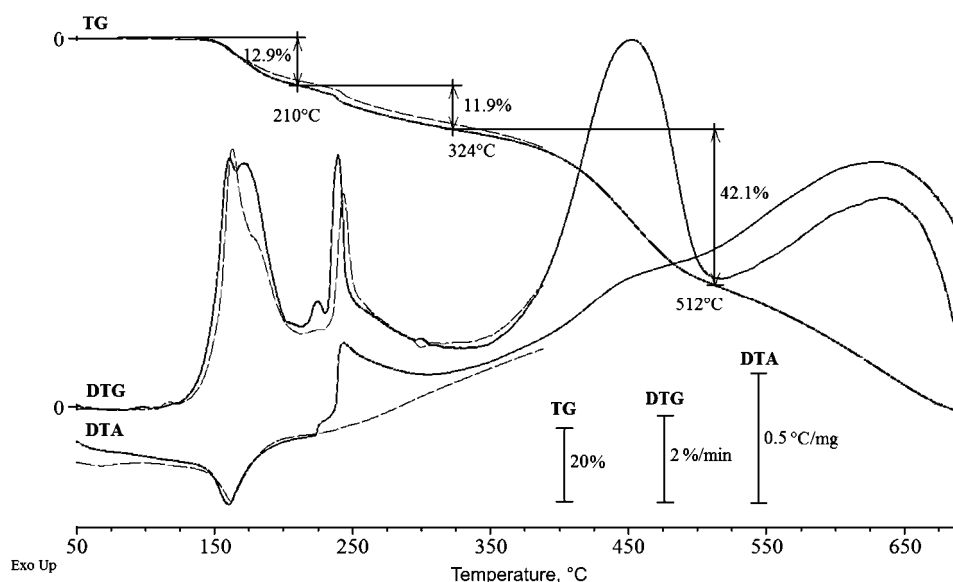


Fig. 5. TG, DTG and DTA curves of the decomposition of $(\text{Haamp})_2[\text{Hg}(\text{SCN})_4]$ in air (—) and in nitrogen (---).

accompanied by the evaporation of the mercury.³³ As there is no stable intermediate formation in the measured temperature range, the course of the decomposition, especially at higher temperatures cannot be explained without additional EGD data. At about 700 °C the decomposition of the compound is accomplished without residue.

The decomposition of Hg(II) complex begins with an endothermic peak in both gas carriers. An additional proof of the organic fragments evaporation is the different shape of DTA curves in air and nitrogen above 200 °C. In air, the DTA curve is asymmetric suggesting the occurrence of multiple processes and the decomposition is highly exothermic. The decomposition in nitrogen is accompanied with a very slightly endothermic process. Above 300 °C the decomposition in both atmospheres is exothermic in the measured range.

Crystallographic data for the structural analysis have been deposited with the Cambridge Crystallographic Data Centre, CCDC No. 736362 and CCDC No.736363 for compounds $[\text{Zn}(\text{NCS})_2(\text{aamp})_2]$ and $(\text{Haamp})_2[\text{Hg}(\text{SCN})_4]$, respectively. Copies of this information may be obtained free of charge from the Director, CCDC, 12 Union Road, Cambridge, CB2 1EZ, UK (fax: +44-1223-336033; e-mail: deposit@ccdc.cam.ac.uk or www: <http://www.ccdc.cam.ac.uk>).

Acknowledgements. The work was financed in part by the Ministry of Science and Technological Development of the Republic of Serbia (Grant No. 142028) and the Provincial Secretariat for Science and Technological Development of Vojvodina. The authors would like to thank Prof. Vladimir Divjaković (Department of Physics, University of Novi Sad, Republic of Serbia) for measuring the crystal data of $[\text{Zn}(\text{NCS})_2(\text{aamp})_2]$.

ИЗВОД

КОМПЛЕКСИ ПРЕЛАЗНИХ МЕТАЛА СА ДЕРИВАТИМА ПИРАЗОЛА.
ДЕО 29. РЕАКЦИЈЕ ЦИНКА(II) И ЖИВА(II) ТИОЦИЈАНАТА СА
4-АЦЕТИЛ-3-АМИНО-5-МЕТИЛПИРАЗОЛОМ

ЖЕЉКО К. ЈАЊИМОВИЋ¹, ГОРАН А. БОГДАНОВИЋ², BERTA HOLLÓ³, ВУКАДИН М. ЛЕОВАЦ³
и KATALIN MÉSZÁROS SZÉCSÉNYI³

¹*Metalurško-tehnološki fakultet, Podgorica, Crna Gora,* ²*Институт за нуклеарне науке "Винча",
Лабораторија за теоријску физику и физику кондензоване материје, Београд и*
³*Природно-математички факултет, Дејарман за хемију, Нови Сад*

Одређене су кристалне и молекулске структуре комплекса цинка(II) и живе(II) са 4-ацетил-3-амино-5-метилпиразолом (aamp) координационих формула $[\text{Zn}(\text{NCS})_2(\text{aamp})_2]$ и $(\text{Haamp})_2[\text{Hg}(\text{SCN})_4]$. Комплекс цинка(II) је добијен реакцијом топлих метанолних раствора смеше цинк(II)-нитрата и амонијум-тиоцијаната са aamp. Комплекс живе(II) настаје у реакцији топлог етанолног раствора aamp и топлог, слабо киселог воденог раствора $[\text{Hg}(\text{SCN})_4]^{2-}$. Оба комплекса имају тетраедарску геометрију, која се у случају комплекса цинка остварује монодентатном координацијом два молекула aamp и две изотиоцијанатне групе. Атоми Zn(II) и Hg(II) налазе се у знатно деформисаном координационом окружењу. У оба комплекса дериват пиразола има планарну форму која је вероватно стабилизована интрамолекулском N–H...O водоничном везом. Добијена једињења су, осим рендгенском структурном

анализом, окарактерисана елементалном анализом, IR-спектрометријом, кондуктометријским мерењима и термичком анализом.

(Примљено 2. јуна, ревидирано 4. октобра 2009)

REFERENCES

1. Y. A. Ivanenkov, K. V. Balakin, S. E. Tkachenko, *Drugs in R and D* **9** (2008) 397
2. M. J. Graneto, R. G. Kurumbail, M. L. Vazquez, Huey-Sheng Shieh, J. L. Pawlitz, J. M. Williams, W. C. Stallings, L. Geng, A. S. Naraian, F. J. Koszyk, M. A. Stealey, X. D. Xu, R. M. Weier, G. J. Hanson, R. J. Mourey, R. P. Compton, S. J. Mnich, G. D. Anderson, J. B. Monahan, R. Devraj, *J. Med. Chem.* **50** (2007) 5712
3. P. E. Almeida da Silva, D. F. Ramosa, H. G. Bonacorso, A. I. de la Iglesia, M. R. Oliveira, T. Coelho, J. Navarini, H. R. Morbidoni, N. Zanatta, M. A. P. Martins, *Int. J. Antimicrob. Agents* **32** (2008) 139
4. E. Reisner, V. B. Arion, B. K. Keppler, A. J. L. Pombeiro, *Inorg. Chim. Acta* **361** (2008) 1569
5. F. P. Pruchnik, P. Jakimowicz, Z. Ciunik, J. Zakrzewska-Czerwińska, A. Opolski, J. Wietrzyk, E. Wojdat, *Inorg. Chim. Acta* **334** (2002) 59
6. K. Sakai, Y. Tomita, T. Ue, K. Goshima, M. Ohminato, T. Tsubomura, K. Matsumoto, K. Ohmura, K. Kawakami, *Inorg. Chim. Acta* **297** (2000) 64
7. G. Lemaire, W. Mnif, J.-M. Pascussi, A. Pillon, F. Rabenoelina, H. Fenet, E. Gomez C. Casellas, J.-C. Nicolas, V. Cavaillès, M.-J. Duchesne, P. Balaguer, *Tox. Sci.* **91** (2006) 501
8. C. B. Vicentini, D. Mares, A. Tartari, M. Manfrini, G. Forlani, *J. Agric. Food Chem.* **52** (2004) 1898
9. N. Singh, N. K. Sangwan, K. S. Dhindsa, *Pest. Manag. Sci.* **56** (2000) 284
10. B. Barszcz, *Coord. Chem. Rev.* **249** (2005) 2259
11. J. Bol, *Ph.D. Thesis*, University Leiden, Leiden, Netherlands, 1997
12. N. E. Schore, *Study Guide and Solutions Manual for Organic Chemistry: Structure and Function*, 5th ed., W. H. Freeman and Company, 2007
13. V. M. Leovac, B. Holló, P. Bombicz, A. Kovács, K. Mészáros Szécsényi, Lj. S. Jovanović, G. Bogdanović, V. Kojić, M. D. Joksović, prepared for publication
14. V. M. Leovac, Z. D. Tomić, K. Mészáros Szécsényi, Lj. S. Jovanović, M. D. Joksović, *J. Serb. Chem. Soc.* **72** (2007) 1281
15. V. Yu. Kukushkin, E. A. Aleksandrova, V. M. Leovac, E. Z. Ivegeš, V. K. Belsky, V. M. Konovalov, *Polyhedron* **20** (1992) 2691
16. A. Hergold-Brundić, B. Kaitner, B. Kamenar, V. M. Leovac, E. Z. Ivegeš, N. Juranić, *Inorg. Chim. Acta* **188** (1991) 151
17. K. Mészáros Szécsényi, V. M. Leovac, Ž. K. Jaćimović, V. I. Češljević, A. Kovács, G. Pokol, S. Gál, *J. Therm. Anal. Cal.* **63** (2001) 723
18. *Enraf-Nonius CAD4 Software*, Version 5.0, Enraf-Nonius, Delft, The Netherlands, 1989
19. *CAD-4 Express Software*, Enraf-Nonius, Delft, The Netherlands, 1994
20. a) A. L. Spek, *Acta Crystallogr. A* **46** (1990) C34; b) A. L. Spek, *PLATON*, A. *Multipurpose: Crystallographic Tool*, Utrecht University, Utrecht, The Netherlands, 1998
21. L. J. Farrugia, *J. Appl. Crystallogr.* **32** (1999) 837
22. A. L. Spek, *J. Appl. Cryst.* **36** (2003) 7
23. *Data collection and processing software*, Version 1, Oxford Diffraction Ltd., Oxford, 2006

24. G. M. Sheldrick, *Acta Crystallogr. A* **64** (2008) 112
25. M. Nardelli, *J. Appl. Crystallogr.* **28** (1995) 659
26. L. J. Farrugia, *J. Appl. Crystallogr.* **30** (1997) 565
27. W. J. Geary, *Coord. Chem. Rev.* **7** (1971) 81
28. K. Nakamoto, *Infrared and Raman Spectra of Inorganic and Coordination Compounds, Part B: Applications in Coordination, Organometallic, and Bioinorganic Chemistry*, 5th ed., Wiley, New York, 1997, p. 116
29. F. H. Allen, *Acta Crystallogr. B* **58** (2002) 380
30. Z. D. Tomić, Ž. K. Jaćimović, V. M. Leovac, V. I. Češljević, *Acta Crystallogr. C* **56** (2000) 777
31. R. G. Pearson, *J. Am. Chem. Soc.* **85** (1963) 3533
32. R. G. Pearson, *J. Chem. Educ.* **64** (1987) 561
33. G. R. Souza, I. A. Pastre, A. V. Benedetti, C. A. Ribeiro, F. L. Fertonani, *J. Therm. Anal. Cal.* **88** (2007) 127.